JOURNAL OF SYNCHROTRON RADIATION

ISSN 1600-5775

X-ray collimation by the parabolic cylinder mirror in SPring-8/BL29XUL

Dai Takei,[a]* Yoshiki Kohmura,[a] Yasunori Senba,[b] Haruhiko Ohashi,[b] Kenji Tamasaku[a] and Tetsuya Ishikawa[a]

[a]RIKEN SPring-8 Center, 1-1-1 Kouto, Sayo, Hyogo 679-5148, Japan, and [b]JASRI, Kouto 1-1-1, Sayo, Hyogo 679-5148, Japan. *Correspondence e-mail: takei@spring8.or.jp

Received 16 May 2015
Accepted 20 October 2015

Edited by A. Momose, Tohoku University, Japan

Keywords: X-ray optics; beam divergence; beamline development.

A combination of plane and threefold-shape X-ray mirrors was installed in SPring-8 BL29XUL. The second mirror has parabolic cylinder surfaces that collimate X-rays in the vertical direction. A performance test was conducted, yielding highly collimated 8 keV photon beams with an effective angular divergence of 0.4 μrad, below only 5% of that of the original beams. The double-mirror system preserved 70% of the total incident flux and nearly tripled the flux density at 988 m from the light source. The values of the observations were almost similar to those of our ray-tracing simulation. Based on the results a discussion of future prospects of the mirror system is included.

1. Introduction

X-ray beam divergence is one of the most important aspects in synchrotron radiation and a foundation of contemporary high-energy photon science. Since the successful launches of third-generation synchrotron facilities and X-ray free-electron lasers, many attempts at precise measurements have been performed with the enormous benefit of their bright, dense, and well collimated X-ray outputs (*e.g.* Miao *et al.*, 2002; Tamasaku *et al.*, 2014; Suga *et al.*, 2015). Further improvement in angular divergence is still important because it leads to an increase in X-ray intensity and, in addition, might enable us to perform ultimate X-ray focusing that should open up a wide variety of nonlinear optical science (*e.g.* Mimura *et al.*, 2010).

Regarding the effective X-ray focusing, current problems are well defined. In order to minimize a focal spot size an X-ray source needs to be highly collimated before entering the collecting optics. Here, a practical way of beam collimation is obtaining enough distance from an optical element to a light source. However, in the course of propagation the light source becomes more widespread over the effective area of an optical element (*e.g.* a grazing-incidence mirror) because of the poor angular divergence. Only a part of the light is focused as a result, yielding no maximum gain of the X-ray intensity at the focal point. We here need to find another approach of X-ray collimation, to go one step further with the knowledge of extremely intense X-rays and related effects.

To solve the problem it can be considered simply to use a parabolic cylinder mirror. This is one of the most traditional approaches of beam collimation, though it has been difficult to achieve superior performance in short-wavelength light because of the necessity of high-quality fabrication. We thus took on a challenge to produce a mirror system with the latest fabrication, and to employ parabolic cylinder optics as a part of the beamline development of BL29XUL in SPring-8

(Ishikawa *et al.*, 2001; Tamasaku *et al.*, 2001); in this paper we demonstrate the performance of our mirror system and discuss its applications.

2. Mirror system

The potential performance of the parabolic cylinder optics was estimated by simulations performed using the ray-tracing code *SHADOW*, version 3 (Sanchez del Rio *et al.*, 2011). In the simulations, an 8 keV monochromatic light source having extended geometrical profile and divergence each with a Gaussian distribution was employed. The Gaussian parameters were estimated using the synchrotron radiation calculation code *SPECTRA*, version 9.0.2 (Tanaka & Kitamura, 2007), and we adopted the values of BL29XUL in SPring-8 of σ_X = 297.87 µm, σ_Z = 6.85 µm in space and $\sigma_{X'}$ = 12.95 µrad, $\sigma_{Z'}$ = 4.30 µrad in divergence, where the subscripts X and X' indicate the horizontal coordinates whereas Z and Z' indicate the vertical coordinates. Optical elements we assumed in the simulations were a 0.5 mm × 0.5 mm slit at 28.9 m and a reflecting mirror that collimates X-ray beams in the vertical plane with an incident angle of 5 mrad. The mirror surface was designed to be a part of the parabolic cylinder that is defined by $y^2 = 4ax$ and $a = r\sin^2\theta \sim 1.21$ mm, where r = 48.5 m is the distance from a focal point to the center of the mirror and θ = 5 mrad is the grazing angle. The angular divergence of the reflected beam depends almost entirely on the source size and the value was expected by the simulations to be 0.3 µrad, more than an order of magnitude smaller than that expected from the original beam of about 9 µrad. Fig. 1(*a*) shows a spot diagram of the collimated beam at 988 m from the light source where it is at the most downstream of BL29XUL. Based on the estimates we produced the mirror system to be installed in the optics hutch of BL29XUL.

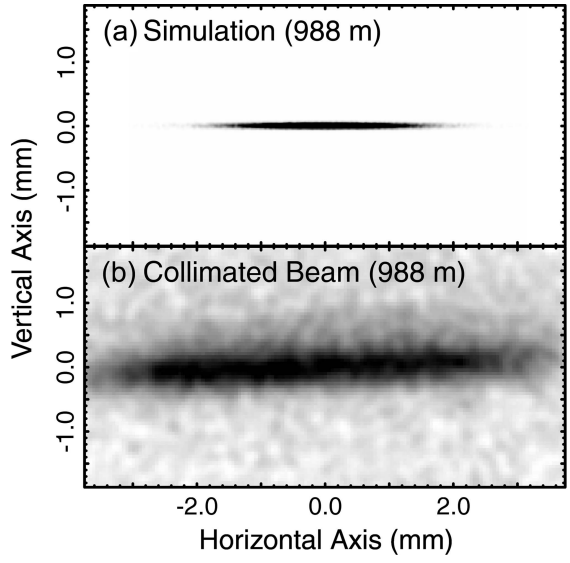

Figure 1
Examples of (*a*) a simulated spot diagram and (*b*) a background-subtracted observed image of a collimated beam at 988 m. Vertical and horizontal axes were shifted by matching the peak position with zero in each image.

Table 1
Parameters of the mirror system in BL29XUL.

	M1	M2
Outer length (mm)	400	400
Outer width (mm)	50	50
Outer thickness (mm)	50	50
Substrate material	Si	Si
Coating material	Rh	Rh
Coating thickness (nm)	100	100
Mirror position (m)	47.4	48.5
Reflection	Upward	Downward

Surface ID	M1-A	M2-A	M2-B	M2-C
Effective length (mm)	~380	~380	~380	~380
Effective width (mm)	~24	~8	~8	~8
Surface shape	Plane	Plane	Parabolic cylinder	Parabolic cylinder
Glancing angle (mrad)	3, 5	3, 5	3	5
RMS figure error (nm)	0.5	0.4	0.3	0.3

The detailed parameters of our mirror system are summarized in Table 1. The first mirror (M1) is a plane (M1-A), while the second mirror (M2) has three regions with different shapes: one plane (M2-A) and two parabolic cylinder (M2-B and M2-C) surfaces. M2-B and M2-C were designed to collimate a point source 48.5 m away at the glancing angles of 3 and 5 mrad, respectively. The mirror substrates are well polished Si, and their surfaces are coated with a 100 nm-thick Rh layer. Machining and coating were performed by JTEC Corporation. Fig. 2 shows the designed surface profiles and the

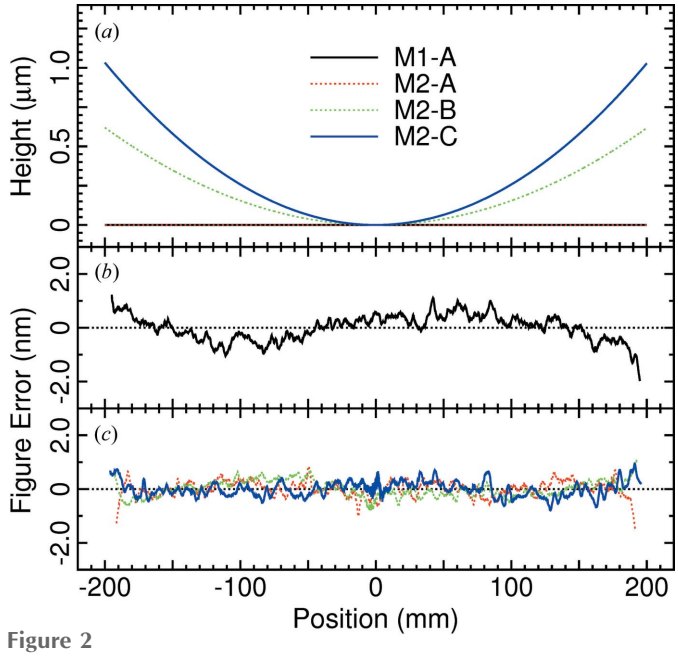

Figure 2
Designed surface profiles (*a*) and the measured figure errors of (*b*) M1 and (*c*) M2 mirrors. The four different surfaces are shown color-coded and the combination in this experiment is shown by the solid lines. The abscissa indicates the longitudinal position from downstream to upstream of the BL29XUL beamline and is shifted by matching the center of the mirror with zero. The figure errors were estimated by profilometry stitching 0.1 mm-width center lines using a combination of *Zygo GPI XP/D* and *NewView7300*.

measured figure errors of M2-B and M2-C. The root mean squares (RMS) of the figure errors are 0.3–0.5 nm, indicating that diffraction-limited optics with the wavefront error better than the $\lambda/4$ level in the useful energy range of BL29XUL (*i.e.* $\lesssim 20$ keV) is achieved. Our emphasis here is focused on demonstrating the collimation performance of the newly installed mirror system by experiment, with a combination of M1-A and M2-C as an example.

3. Experiment

3.1. Set-up

The collimation performance of the mirror system was then evaluated at BL29XUL in SPring-8. The beamline BL29XUL consists of an in-vacuum magnetic undulator, an optics hutch and four experimental stations along with 1 km vacuum pipes. The undulator gap is adjustable in the range 8–50 mm, yielding a photon beam with an energy spectral peak in about 5–20 keV. It has to be noted that a beam divergence is commonly measured by rotating an analyzer crystal but this approach cannot be employed in our case. This is because the expected measurements of order sub-μrad are significantly smaller than the angular acceptance of a Bragg reflection with an effective lattice plane of a common crystal. We thus utilized the extremely long transport channel in BL29XUL and derived the beam divergences directly from the geometric spreading of the X-ray beams as a function of the distance of travel.

Fig. 3 shows the experimental set-up of this study. X-rays were generated by the undulator with a 12.55 mm gap, yielding the peak intensity at 8 keV. Then the beams were shaped by the 0.5 mm × 0.5 mm front-end (FE) slit at 28.9 m from the light source (Oura *et al.*, 1998). The double-crystal Si(111) monochromator (DCM) at 43.2 m was used to extract 8 keV beams. M1-A and M2-C mirrors were installed at 47.4 and 48.5 m to reflect beams upward and downward, respectively. The incident angles of M1-A and M2-C were both at 5 mrad. The beams passed through the 4 mm × 4 mm transport-channel (TC) slit at 50.3–50.6 m. X-ray intensity was measured by a temporarily installed photodiode at 52.5 m and ionization chambers; the beam-intensity loss by the additions of the mirror system was measured to be 30%.

For the sake of adjusting the collimated-beam positions to the original axis, the 400 reflections of a channel-cut Si(100) crystal (CCC) were used at 61.3 m. X-ray images were obtained by the two sets of a phosphor-coupled beam monitor (BM) and a Hamamatsu Photonics ORCA-R2 CCD camera at 65 or 988 m from the light source. The optical paths between the above elements were bridged by vacuum pipes as long as possible, and the whole air-path lengths from the light source to the CCD cameras at 65 and 988 m were reduced to about 2 and 3 m, respectively.

In the experiment, a total of four image sets were obtained. Two of them were original beams and the remaining two were collimated beams, each at 65 and 988 m from the light source. One data set includes 2000 sequential background-subtracted X-ray images each with a CCD exposure time of 10 μs; the short snapshots minimized beam spreading of the vibration of the beamline optics. Fig. 1(*b*) shows an example of a background-subtracted image of a collimated beam at 988 m. The data acquisitions were performed during 1–2 October 2013, when the fluctuation of the beam current of the SPring-8 electron storage ring was controlled below $\lesssim 0.1\%$.

3.2. DuMond diagram

We here confirmed the angular characteristics of the existing beamline optics. Fig. 4 is an expected DuMond diagram that shows the angular acceptances of the optical elements, except for the newly installed mirror system and the substantially large TC slit. The angle–wavelength plane of the light source of BL29XUL was also calculated using the *SPECTRA* code. The Darwin widths of the Bragg reflections of the crystals were approximated as

$$\omega = \frac{2r_e\lambda^2|f_g|}{\pi v_c \sin 2\theta_B}, \tag{1}$$

where r_e is the classical electron radius, λ is the wavelength, f_g is the structure factor, v_c is the unit-cell volume of a crystal and θ_B is the Bragg reflection angle (Darwin, 1914*a*,*b*). r_e can be adopted from the NIST database (Mohr *et al.*, 2012) and f_g is derived from the DABAX files in the *XOP* software (Kissel, 2000; Sanchez del Rio & Dejus, 2004). The resulting diagram indicates that the optical elements other than the mirror system have little or almost no effect on the angular diver-

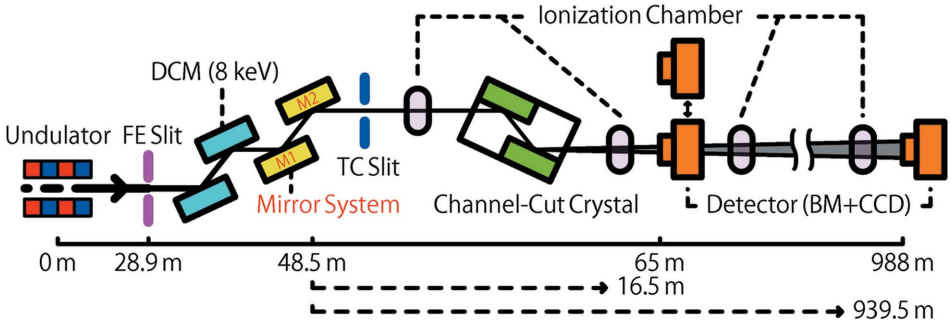

Figure 3
Schematic view of the experimental set-up. The original beams of 8 keV X-rays were led by the FE slit and the DCM to the collimation mirror system and their output were monitored by the ionization chambers and detected using the phosphor-coupled CCD cameras. The bottom rulers and labels indicate the distances to each element from the undulator light source, and to the CCD cameras from the second mirror.

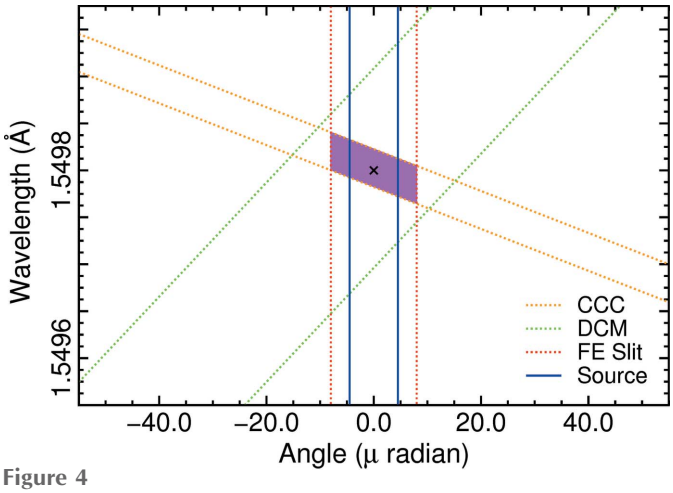

Figure 4
Angular acceptances of the optical elements are shown color-coded, namely a DuMond diagram of this experiment. The magenta area indicates the total acceptance of the combination of the FE slit, the DCM and the CCC, suggesting that these elements have no significant role in the divergence angles of the original light source (blue). We were therefore able to observe the pure contribution of the remaining element, *i.e.* the newly installed mirror system, in this experiment.

gence of the light source, meaning that the mirror system should be accountable for the beam collimation in this experiment.

4. Analysis and results

We extracted vertical X-ray profiles from the four sets of 2000 sequential images, and then fitted each data with a Gaussian and constant model. Fig. 5 shows examples of the background-subtracted profiles at 65 and 988 m; the collimated beams were able to keep their profiles narrow even at 988 m. The peak

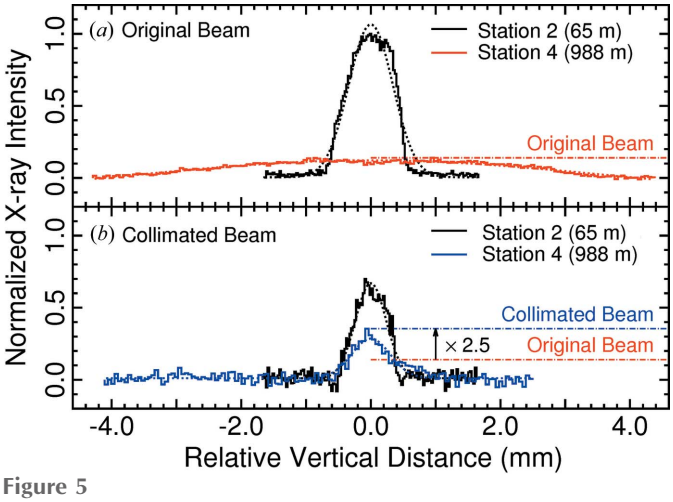

Figure 5
Comparisons of vertical profiles of original (*a*) and collimated (*b*) beams taken at 65 and 988 m, respectively, from the undulator light source. The dashed lines indicate the best-fit models, consisting of Gaussian and constant components. Each profile is normalized to a maximum of that of the data taken at 65 m, and then in (*b*) the values were corrected for the throughput of the mirror system. The dash-dotted line indicates the peak values of the original and collimated beams each at 988 m.

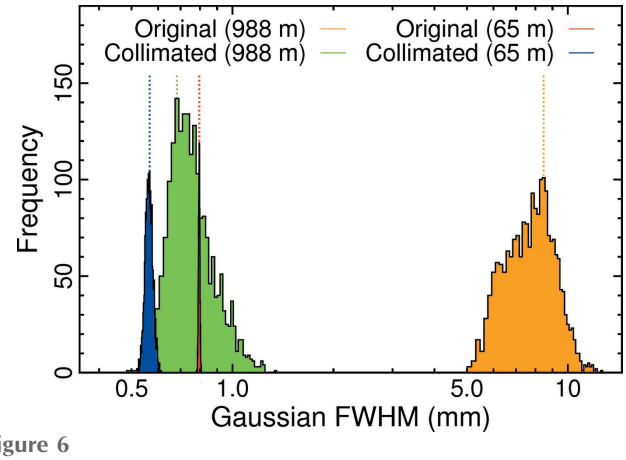

Figure 6
Histograms of Gaussian FWHM values obtained from model fits to 2000 vertical beam profiles taken with the four different conditions; the data of the original and reflected beams at each distance are shown color-coded. The dashed lines indicate the mode values of each histogram, which we chose as working hypothesis values of typical beam sizes.

intensities of the original and collimated beams at 988 m were derived to be 14 and 51%, respectively, of their values taken at 65 m. After taking into account the 30% intensity loss due to the mirror system, the results indicate that the flux density at 988 m was increased by a factor of 2.5. Typical beam sizes in the vertical direction were further estimated from the histograms of the Gaussian widths of each sequential image; the mode values were 0.80 and 8.47 mm for the original beams and 0.57 and 0.68 mm for the collimated beams in the full width at half-maximum (FWHM) at 65 and 988 m, respectively (Fig. 6).

5. Discussion

5.1. Angular divergence

The observed beam size (S_O) is simply approximated by

$$S_O \sim \left[S_S^2 + \left(D_A \times L_P\right)^2\right]^{1/2}, \qquad (2)$$

where S_S is the source size, D_A is the angular divergence and L_P is the path length. Assuming S_S is constant, D_A is derived from the two sets of S_O and L_P. Adopting S_O = 0.57 mm and 0.68 mm at L_P = 16.5 m and 939.5 m, respectively, an effective D_A of the reflected beam is derived to be 0.4 μrad. In the same way as for the original beam D_A is 9.0 μrad; the values indicate that the angular divergence was significantly improved by using the mirror system, and was almost comparable to that of the ray-tracing simulations.

5.2. Progress and future prospects

Difficulties in X-ray collimation are primarily due to the loss of beam intensity. A traditional approach is the use of asymmetric Bragg reflections, which improve the beam divergence dramatically (Ishikawa, 1989; Ishikawa *et al.*, 1991; Brauer *et al.*, 1995), at the expense of a significant part of the flux. Another choice we have is an X-ray refractive lens that provides high efficiency and usability with a typical angular

divergence of the order of μrad (Snigirev *et al.*, 1996; Baron *et al.*, 1999). This paper shows an additional approach of achromatic X-ray collimation using the parabolic cylinder mirror system, which yields both about 70% throughput and the sub-μrad angular divergence. Further progress in this direction might expect to provide greater opportunities of forthcoming studies requesting the high-quality beams; *e.g.* ultra-small-angle X-ray scattering (Bonse & Hart, 1966), X-ray holography (Cloetens *et al.*, 1999) and the gravitational red-shift measurement by an extremely long X-ray interferometer (Ishikawa *et al.*, 2001).

6. Summary

The combination of plane and threefold-shape mirrors was installed in the optics hutch of BL29XUL in SPring-8. The second mirror has parabolic cylinder surfaces that allow the light source in the vertical direction to be collimated. We conducted a performance test, yielding highly collimated 8 keV photon beams with an effective angular divergence of 0.4 μrad, below only 5% of that of the original light source. The value is slightly larger than but almost comparable to that of the ray-tracing simulations. This experiment becomes a rare example of representing the collimation utility of the parabolic cylinder mirror in X-ray optics and our approach would be helpful in the design of future experiments and of beamline developments.

Acknowledgements

This research has made use of experimental data obtained by the RIKEN/BL29XUL beamline in SPring-8. The authors express gratitude to RIKEN for allocating a part of beam times for our research and to JASRI for operating SPring-8. We thank H. Yamazaki, T. Wagai and M. Yamamoto for valuable discussions and support. DT acknowledges financial support by the Special Postdoctoral Researchers Program in RIKEN.

References

Baron, A. Q. R., Kohmura, Y., Ohishi, Y. & Ishikawa, T. (1999). *Appl. Phys. Lett.* **74**, 1492.
Bonse, U. & Hart, M. (1966). *Z. Phys.* **189**, 151–162.
Brauer, S., Stephenson, G. B., Sutton, M., Mochrie, S. G. J., Dierker, S. B., Fleming, R. M., Pindak, R., Robinson, I. K., Grübel, G., Als-Nielsen, J. & Abernathy, D. L. (1995). *Rev. Sci. Instrum.* **66**, 1506–1509.
Cloetens, P., Ludwig, W., Baruchel, J., Van Dyck, D., Van Landuyt, J., Guigay, J. P. & Schlenker, M. (1999). *Appl. Phys. Lett.* **75**, 2912.
Darwin, C. G. (1914*a*). *Philos. Mag.* **27**, 315–333.
Darwin, C. G. (1914*b*). *Philos. Mag.* **27**, 675–690.
Ishikawa, T. (1989). *Rev. Sci. Instrum.* **60**, 2490–2493.
Ishikawa, T., Hirano, K. & Kikuta, S. (1991). *Nucl. Instrum. Methods Phys. Res. A*, **308**, 356–362.
Ishikawa, T., Tamasaku, K., Yabashi, M., Goto, S., Tanaka, Y., Yamazaki, H., Takeshita, K. T., Kimura, H., Ohashi, H., Matsushita, T. & Ohata, T. (2001). *Proc. SPIE*, **4145**, 1–10.
Kissel, L. (2000). *Radiat. Phys. Chem.* **59**, 185–200.
Miao, J., Ishikawa, T., Johnson, B., Anderson, E. H., Lai, B. & Hodgson, K. O. (2002). *Phys. Rev. Lett.* **89**, 088303.
Mimura, H., Handa, S., Kimura, T., Yumoto, H., Yamakawa, D., Yokoyama, H., Matsuyama, S., Inagaki, K., Yamamura, K., Sano, Y., Tamasaku, K., Nishino, Y., Yabashi, M., Ishikawa, T. & Yamauchi, K. (2010). *Nat. Phys.* **6**, 122–125.
Mohr, P. J., Taylor, B. N. & Newell, D. B. (2012). *Rev. Mod. Phys.* **84**, 1527–1605.
Oura, M., Sakurai, Y. & Kitamura, H. (1998). *J. Synchrotron Rad.* **5**, 606–608.
Sanchez del Rio, M., Canestrari, N., Jiang, F. & Cerrina, F. (2011). *J. Synchrotron Rad.* **18**, 708–716.
Sanchez del Rio, M. & Dejus, R. J. (2004). *Proc. SPIE*, **5536**, 171–174.
Snigirev, A., Kohn, V., Snigireva, I. & Lengeler, B. (1996). *Nature (London)*, **384**, 49–51.
Suga, M., Akita, F., Hirata, K., Ueno, G., Murakami, H., Nakajima, Y., Shimizu, T., Yamashita, K., Yamamoto, M., Ago, H. & Shen, J. R. (2015). *Nature (London)*, **517**, 99–103.
Tamasaku, K., Shigemasa, E., Inubushi, Y., Katayama, T., Sawada, K., Yumoto, H., Ohashi, H., Mimura, H., Yabashi, M., Yamauchi, K. & Ishikawa, T. (2014). *Nat. Photon.* **8**, 313–316.
Tamasaku, K., Tanaka, Y., Yabashi, M., Yamazaki, H., Kawamura, N., Suzuki, M. & Ishikawa, T. (2001). *Nucl. Instrum. Methods Phys. Res. A*, **467–468**, 686–689.
Tanaka, T. & Kitamura, H. (2007). *AIP Conf. Ser.* **879**, 355–358.